Proceedings of the ASME 2010 3rd Joint US-European Fluids Engineering Summer Meeting and 8th International Conference on Nanochannels, Microchannels, and Minichannels
FEDSM-ICNMM2010
August 1-5, 2010, Montreal, Canada

FEDSM-ICNMM2010-31101

NUMERICAL ANALYSIS OF THE CONJUGATED HEAT TRANSFER PROBLEM FOR MIXED ELECTRO-OSMOTIC AND PRESSURE-DRIVEN FLOWS OF PHAN-THIEN TANNER FLUIDS IN MICROCHANNELS

Juan P. Escandón, Oscar E. Bautista
SEPI-ESIME Unidad Azcapotzalco, Departamento de Termofluidos
México D.F., México, 02550
++ (52) 55 5729 6000, Ext. 64487, jescandon@ipn.mx

Federico Méndez
Facultad de Ingeniería, UNAM, Departamento de Termofluidos
México D. F., México, 04510, fmendez@servidor.unam.mx

ABSTRACT
In this work we solve numerically the conjugated heat transfer problem of a non-Newtonian fluid and solid walls in a microchannel under the influence of pressure and electro-osmotic forces. The velocity field is determined taking into account a hydrodynamically fully-developed flow and a constitutive relation based in a viscoelastic rheological model with a simplified Phan-Thien Tanner fluid. The numerical process results in solid and fluid temperature distributions. Is shown the influence of nondimensional parameters involved in the analysis on the conjugated heat transfer problem: an indicator of viscoelastic behavior, the Peclet number, a normalized power generation term being the ratio of heat flow from the external wall to the Joule heating, a conjugation term which determines the basic heat transfer regimes between fluid and solid sections in the microchannel. For the flow field: the ratio of pressure forces to the electro-osmotic forces acts on flow as a drag reducer and drag increaser under favorable and adverse pressure gradients, respectively, moreover, for increasing values of the viscoelastic parameter, the velocity of the fluid increases with respect the Newtonian fluid flow case. These velocity perturbations resulting in cross-sectional variations of temperature.

Keywords — Electro-osmotic, Phan Thien Tanner fluid, conjugate heat transfer, microchannel.

INTRODUCTION
The microfluidic devices are used in the handling of biomedical and chemical analysis. Thus, electrokinetic transport is widely used to control flow and for manipulate sample solutes, include injection, separation, mixing, dilution/concentration, and reaction. Originally, the electrokinetic transport operates a combination of two mechanisms drivers: electrophoresis and electro-osmosis. Electrophoresis is the migration of charged solutes (e.g. ions, macromolecules of DNA) in an electrolyte under an applied electric field. The electro-osmosis gives the movement of a volume of an aqueous solution adjacent to a solid charged surface when an external electric field is applied tangentially along the surface [1]. Due to the rapid development of "Lab-on-a-Chip" technologies during recent years, electro-osmosis is being used extensively as a driving force for manipulating fluid flows for transport and control samples in nano volumes of fluids to biological, chemical and medical diagnostics. Advances in microfluidic devices make possible a complete analysis of fluids in the biochemistry area in a single fabricated chip; therefore, is fundamental understand the characteristics of fluids flow in microchannels to have an optimum design and precise control of microfluidics devices [2].

The physics of electrokinetic phenomena and specifically in the electro-osmotic and electrophoretic flow has been reviewed extensively in the literature. The fundamental hydrodynamic of electro-osmotic and electrophoretic flow is detailed by Masliyah, Karniadaski and Li [3-5]. The heat transfer phenomena in microchannels has been studied by Xuan, [6, 7], and Tang [1, 8, 9], they analyze the coupled cases with temperature and conjugates problems in electro-osmotic flow, and is emphasized the inevitable effect of Joule heating in the flow.

The separation of samples species by electrophoretic flow based only over the solvent fluid in microchannels is treated by Tang [1, 9, 10] and Xuan [11]. Such works in this paragraph are under consideration of Newtonian fluids, its only considers the part of the solvent in the flow, and some are in transient state.

So, with the advent of electrokinetics for the transport of biological fluids through biochips, is necessary to mathematically characterize the transport mechanisms associated with the process for efficient design of microfluidic systems. Strategies for characterization are based on electro-osmotic transport of Newtonian fluids, however, that consideration may be somewhat inappropriate for these applications. It´s clear that a model such as Newton's law of viscosity may be insufficient to fully describe the constitutive behavior of biological fluids complex. Although in the literature there are several models proposed to analyze the behavior of non Newtonian fluids, at present, still appear relevant implications on the transport of electrokinetic flows that have not been completely resolved by the scientific community [12]. Studies by Zhao, Berli and Tang [13-15] in this regard consider the power law for non Newtonian fluids and solve only the hydrodynamics of electro-osmotic flow; Das [12] also uses the power law to solve analytically the distribution of velocity, temperature and concentration on electro-osmotic flows of non Newtonian biological fluids; Park [16] presents a hydrodynamics investigation for electro-osmotic flow of viscoelastic fluids as blood and DNA through microchannels, where is adapted the concept of the Helmholtz-Smoluchowski velocity for viscoelastic fluids. An analytical solution has been presented by Alfonso [17] for the flow of viscoelastic fluids in steady state and fully developed flow in microchannels of parallel plates and pipes under the influence of pressure and electrokinetic forces using the Debye-Hückel approximation, this work shows the combined effects of the rheology of the fluid and the gradients of electro-osmotic and pressure forces on the velocity distribution; the viscoelastic fluids employees describe the constitutive Phan-Thien Thaner model, and is an approximation of studies of fluids such as blood, saliva, synovial and other biofluids. The studies mentioned above are developed in a steady state.

METHODOLOGY

A. Physical model

The Figure 1 shows a squematic view of the physical model, the fluid flow is through of a microchannel formed by two parallel flat plates of height $2H$, length L, and width w, the wall thickness is H_w. $L/H \gg 1$, $L/H_w \gg 1$, $w/H \gg 1$, $w/H_w \gg 1$. We considered a viscoelastic fluid with a simplified Phan-Thien Tanner model. The driving forces are provided by an electric field E_x and a pressure gradient p_x in the axial direction between inlet and outlet of microchannel. For analysis, properties are considered constant with the temperature, the heat transfer is in steady state and flow hydrodynamically developed. The fluid enters at a temperature T_e in $x = 0$. The wall has adiabatic conditions in $x \le 0$ and $x \ge L$. To $0 \le x \le L$ there is a constant heat flux q_0'' in the external wall.

B. Energy equations

The energy equation in the fluid is given by

$$\rho C_{pf} u \frac{\partial T}{\partial x} = k_f \frac{\partial^2 T}{\partial x^2} + k_f \frac{\partial^2 T}{\partial y^2} + \sigma E_x^2 \qquad (1)$$

where $\rho, C_{pf}, T, k_f, \sigma$ and u are the density, the specific heat, the temperature, the thermal conductivity, the electrical conductivity and the axial velocity component of the fluid respectively; x, y are the axial and the transversal coordinate. The boundary conditions associated with equation (1) are

$$\begin{gathered} x = 0 : T = T_e \\ x = L : \partial T/\partial x = 0 \\ y = 0 : \partial T/\partial y = 0, \\ y = H : T_w = T; -k_w \left(\partial T_w/\partial y\right) = -k_f \left(\partial T/\partial y\right) \end{gathered} \qquad (2)$$

where T_w, and k_w are the temperature and the thermal conductivity in the wall respectively.

The energy equation in the solid is given by

$$\frac{\partial^2 T_w}{\partial x^2} + \frac{\partial^2 T_w}{\partial y^2} = 0 \qquad (3)$$

and the boundary conditions associated with equation (3) are

$$\begin{gathered} x = 0 : \partial T_w/\partial x = 0 \\ x = L : \partial T_w/\partial x = 0 \\ -k_w \left(\partial T_w/\partial y\right)\big|_{y=H+H_w} = q_0'' \\ y = H : T_w = T; -k_w \left(\partial T_w/\partial y\right) = -k_f \left(\partial T/\partial y\right) \end{gathered} \qquad (4)$$

Defining the following dimensionless variables

$$\begin{gathered} \chi = x/L \\ \eta = y/H \\ \bar{u} = u/u_{HS} \\ \theta = k_f \left(T - T_e\right)\big/ \sigma E_x^2 H^2 \\ \theta_w = k_f \left(T_w - T_e\right)\big/ \sigma E_x^2 H^2 \\ Z = \left(y - H\right)/H_w \end{gathered} \qquad (5)$$

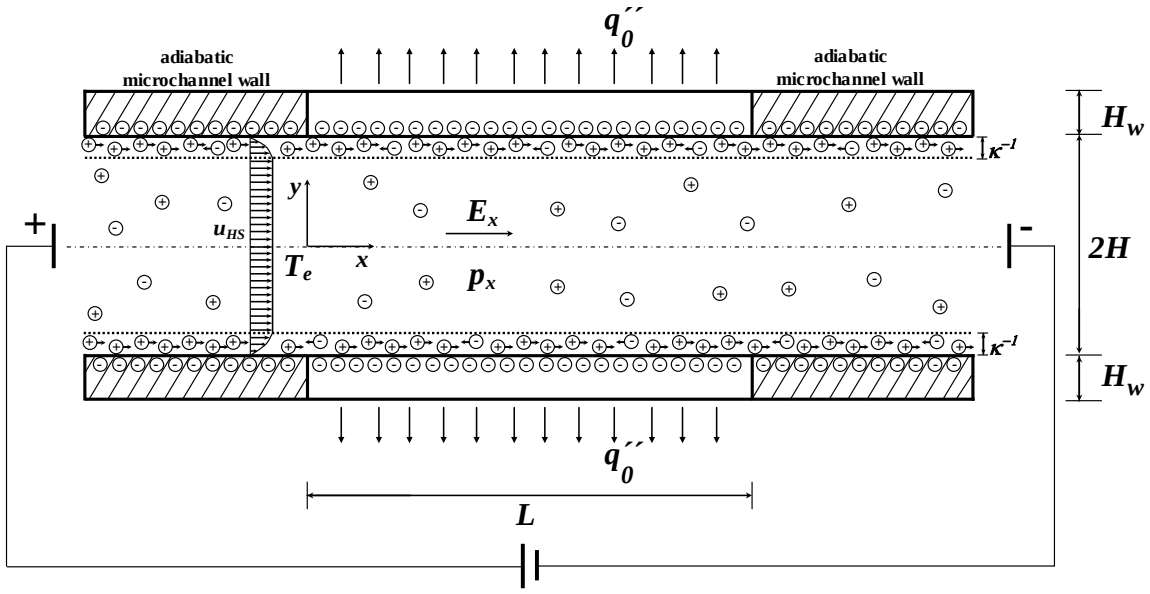

FIG. 1 SCHEMATIC OF MIXED ELECTRO-OSMOTIC AND PRESSURE DRIVEN FLOW BETWEEN TWO PARALLEL FLAT PLATES.

where χ and η are the dimensionless axial and the transversal coordinates respectively; $\bar{u}$, θ, θ_w and Z are the velocity, the temperature in the fluid, the temperature in the solid and the transversal coordinate to analyze the solid wall, dimensionless, respectively. $u_{HS} = -\in \zeta E_x/\eta_0$ [17] is the electro-osmotic reference Helmholtz - Smoluchowski velocity; $\in, \zeta, \eta_0$ are the dielectric constant, the Zeta potential in the shear plane of the double electric layer (EDL) and the apparent viscosity of the fluid, respectively. By introduce the dimensionless variables from equation (5) in equations (1-2) is obtained the dimensionless energy equation to the fluid region into microchannel

$$\beta Pe\bar{u}\frac{\partial\theta}{\partial\chi} = \beta^2\frac{\partial^2\theta}{\partial\chi^2} + \frac{\partial^2\theta}{\partial\eta^2} + 1 \tag{6}$$

and their boundary conditions

$$\begin{gathered}\chi = 0: \theta = 0 \\ \chi = 1: \partial\theta/\partial\chi = 0 \\ \eta = 0: \partial\theta/\partial\eta = 0 \\ \eta = 1: \theta = \theta_w\end{gathered} \tag{7}$$

in addition to equation (7) was considered the next boundary condition in the internal interface of microchannel

$$\bar{\alpha}\frac{\beta^2}{\bar{\varepsilon}^2}\frac{\partial\theta_w}{\partial Z}\bigg|_{Z=0} = \frac{\partial\theta}{\partial\eta}\bigg|_{\eta=1} \tag{8}$$

The energy equation in the fluid and their boundary conditions leaves the following dimensionless parameters

$$\begin{gathered}\beta = H/L \\ \bar{\varepsilon} = H_w/L \\ Pe = \rho C_{pf} u_{HS} H/k_f \\ \bar{\alpha} = \left(k_w/k_f\right)(H/L)(H_w/L)\end{gathered} \tag{9}$$

where β and $\bar{\varepsilon}$ are the aspect ratios in the fluid and solid region, respectively; Pe and $\bar{\alpha}$ are the Peclet number and the conjugation term which determines the basic heat transfer regimes between fluid and solid sections in the microchannel.

Equation (6) implies the viscoelastic properties of the fluid in the dimensionless model of velocity, taking into account the rheological simplified Phan-Thien Tanner model with the electrokinetic and pressure forces in the fluid flow [17]. So, the dimensionless model of velocity is given by

$$\begin{aligned}\bar{u} = &\left(1-2D\varepsilon De_\kappa^2\right)\left(1-F\right) + \frac{2}{3}\varepsilon De_\kappa^2\left(1-F^3\right) - \\ &\frac{1}{2}\Gamma\left(1-\eta^2\right)\left[1+\frac{\varepsilon De_\kappa^2}{\bar{\kappa}^2}\Gamma^2\left(1+\eta^2\right)\right] + \\ &\frac{3}{2}\frac{\varepsilon De_\kappa^2}{\bar{\kappa}^2}\Gamma\left[1-F^2+\left(\bar{\kappa}^2-\left(\bar{\kappa}\eta\right)^2\right)D+2\bar{\kappa}M\left(\eta FR-1\right)\right] - \\ &\frac{12\varepsilon De_\kappa^2}{\bar{\kappa}^4}\Gamma^2\left[\bar{\kappa}M\left(1-\eta R\right)+\left(1+\frac{1}{2}\left(\bar{\kappa}\eta\right)^2\right)F-\left(1+\frac{1}{2}\bar{\kappa}^2\right)\right]\end{aligned} \tag{10}$$

where

$$\Gamma = -H^2 p_x/\in \zeta E_x$$

$$De_{\kappa} = \lambda_1 \kappa u_{HS}$$
$$\bar{\kappa} = \kappa H$$
$$D = 1/\cosh^2(\bar{\kappa})$$
$$M = \tanh(\bar{\kappa})$$
$$F = \cosh(\bar{\kappa}\eta)/\cosh(\bar{\kappa})$$
$$R = \sinh(\bar{\kappa}\eta)/\sinh(\bar{\kappa}) \quad (11)$$

where Γ, De_{κ}, ε, κ, λ_1 and $\bar{\kappa}$ are the ratio of pressure forces on electro-osmotic forces, the Deborah number, the coefficient of elongacional viscosity of the fluid, the inverse Debye length, the relaxation time, and electrokinetic parameter, respectively; *D*, *M*, *F*, and *R* are parameters to simplify.

From equation (5) and (9) in equations (3-4) is obtained the dimensionless energy equation to the solid region in the microchannel

$$\bar{\alpha}\frac{\partial \theta_w}{\partial \chi^2} + \frac{\bar{\alpha}}{\bar{\varepsilon}^2}\frac{\partial^2 \theta_w}{\partial Z^2} = 0 \quad (12)$$

and their boundary conditions

$$\chi = 0 : \partial\theta_w/\partial\chi = 0$$
$$\chi = 1 : \partial\theta_w/\partial\chi = 0$$
$$\theta = \theta_w \ en \ Z = 0 \quad (13)$$

In addition to equation (13) was considered the next boundary condition in the external interface of microchannel

$$\left.\frac{\partial \theta_w}{\partial Z}\right|_{Z=1} = -\frac{\bar{\varepsilon}^2}{\bar{\alpha}}\Lambda \quad (14)$$

where

$$\Lambda = q_0''/\sigma E_x^2 H \quad (15)$$

Λ is the normalized power generation term being the ratio of heat flux from the external wall to the Joule heating. In addition to equation (13) was considered the boundary condition marked by the equation (8) in the internal interface of the microchannel wall.

C. Numerical solution

The previous mathematical model was discretized in central finite differences and solved by the iterative method Successive-Over-Relaxation (SOR) [18]. In the SOR method, the temperature is evaluated in successive iterations by

$$\theta_{i,j}^{k+1} = \theta_{i,j}^{k} + \varpi\Delta\theta_{i,j}^{k+1} \quad (16)$$

where i, j are the nodal positions in axial and transversal direction; k, ϖ and $\Delta\theta_{i,j}^{k+1}$ are the iteration number, the relaxation factor in the SOR method and the dimensionless temperature variation per iteration and node of the discretized mesh, respectively. Equation (16) is applicable for the solid and fluid regions.

Fluid region: $\theta_{i,j}^{k+1}$ is analyzed for the fluid region as follows. The temperature variation of the interiors nodes that not correspond to boundary nodes was determined by

$$\Delta\theta_{i,j}^{k+1} = \left\{ \begin{array}{l} \left[\beta^2 - \frac{\Delta\chi\beta Pe\bar{u}_j}{2}\right]\theta_{i+1,j} + \Omega^2\theta_{i,j+1} + \\ \left[\beta^2 + \frac{\Delta\chi\beta Pe\bar{u}_j}{2}\right]\theta_{i-1,j} + \Omega^2\theta_{i,j-1} - \\ 2\left(\beta^2 + \Omega^2\right)\theta_{i,j} + \Delta\chi^2 \end{array} \right\} \Big/ 2\left(\beta^2 + \Omega^2\right) \quad (17)$$

where $\Omega = \Delta\chi/\Delta\eta$ is the aspect ratio of the discretized mesh for the fluid region; $\Delta\chi$ and $\Delta\eta$ are the increments in the axial and transversal direction respectively. For the dimensionless velocity $\bar{u}_j$ in the equation (10), η is replaced by $\eta_j = j\Delta\eta$.

The specified temperature in the inlet of microchannel, as boundary condition is from equation (7) is

$$\theta(i,j) = 0, \ \text{for} \ i = 0, j = 0 \ \text{to} \ jmax \quad (18)$$

where $jmax$, is the maximum number of nodes in the transversal coordinate.

The boundary conditions in the fluid region which are not specified temperature were adapted to the SOR method as follows; for the boundary condition at the outlet of microchannel gives

$$\Delta\theta_{i,j}^{k+1} = \left\{ \begin{array}{l} \Omega^2\theta_{i,j+1} + 2\beta^2\theta_{i-1,j} + \Omega^2\theta_{i,j-1} \\ -2\left(\beta^2 + \Omega^2\right)\theta_{i,j} + \Delta\chi^2 + \\ \left[\beta^2 - \frac{\Delta\chi\beta Pe\bar{u}_j}{2}\right]2\Delta\chi F_{x2} \end{array} \right\} \Big/ 2\left(\beta^2 + \Omega^2\right) \quad (19)$$

where $F_{x2} = \left(\partial\theta/\partial\chi\right)\big|_{\chi=1} = 0$; for $i = imax$; $j = 1$ to $jmax$-*1*. $imax$ is the maximum number of nodes in the axial coordinate.

The boundary condition at the center of microchannel gives

$$\Delta\theta_{i,j}^{k+1}=\left\{\begin{array}{l}\left[\beta^2-\dfrac{\Delta\chi\beta Pe\bar{u}_j}{2}\right]\theta_{i+1,j}+2\Omega^2\theta_{i,j+1}+\\ \left[\beta^2+\dfrac{\Delta\chi\beta Pe\bar{u}_j}{2}\right]\theta_{i-1,j}-\\ 2\left(\beta^2+\Omega^2\right)\theta_{i,j}+\Delta\chi^2-2\Omega^2\Delta\eta F_{y1}\end{array}\right\}\Bigg/2\left(\beta^2+\Omega^2\right) \qquad (20)$$

where $F_{y1}=\left(\partial\theta/\partial\eta\right)\big|_{\eta=0}=0$, for $j=0; i=1$ to *imax - 1.*

The specified temperature in the internal interface of microchannel as boundary condition is from equation (7) is

$$\theta(i,j)=\theta_w(i,j), \text{ for } j=jmax, i=0 \text{ to } imax. \qquad (21)$$

In addition, to the boundary condition at the internal interface of microchannel requires an equation to solve the boundary nodes, from equation (8) is obtained

$$\Delta\theta_{i,j}^{k+1}=\left\{\begin{array}{l}\left[\beta^2-\dfrac{\Delta\chi\beta Pe\bar{u}_j}{2}\right]\theta_{i+1,j}+2\Omega^2\theta_{i,j-1}+\\ \left[\beta^2+\dfrac{\Delta\chi\beta Pe\bar{u}_j}{2}\right]\theta_{i-1,j}-\\ 2\left(\beta^2+\Omega^2\right)\theta_{i,j}+\Delta\chi^2+2\Omega^2\Delta\eta F_{y2(i,j)}\end{array}\right\}\Bigg/2\left(\beta^2+\Omega^2\right) \qquad (22)$$

where $F_{y2(i,j)}=\bar{\alpha}\dfrac{\beta^2}{\bar{\varepsilon}^2}\dfrac{\partial\theta_{w,i,j}}{\partial Z}\Big|_{Z=0}$ for $j=jmax, i=1 \text{ to } imax - 1.$

The boundary conditions in the corner nodes $i=imax,\ j=0$ and $i=imax,\ j=jmax$ are respectly adapted to the SOR method.

Solid region: $\theta_{i,j}^{k+1}$ is analyzed for the solid region as follows. The temperature variation of the interiors nodes that not correspond to boundary nodes was determined by

$$\Delta\theta_{w,i,j}^{k+1}=\left\{\begin{array}{l}\bar{\alpha}\theta_{w,i+1,j}+\dfrac{\bar{\alpha}}{\bar{\varepsilon}^2}\Phi^2\theta_{w,i,j+1}+\bar{\alpha}\theta_{w,i-1,j}+\\ \dfrac{\bar{\alpha}}{\bar{\varepsilon}^2}\Phi^2\theta_{w,i,j-1}-2\bar{\alpha}\left(1+\dfrac{\Phi^2}{\bar{\varepsilon}^2}\right)\theta_{w,i,j}\end{array}\right\}\Bigg/2\bar{\alpha}\left(1+\frac{\Phi^2}{\bar{\varepsilon}^2}\right) \qquad (23)$$

where $\Phi=\Delta\chi/\Delta Z$, is the aspect ratio of the discretized mesh for the solid region; ΔZ is the increment in the transverse direction.

Boundary conditions in the solid region which are not specified temperature were adapted to the SOR method as follows; the boundary condition at the left side of the microchannel wall gives

$$\Delta\theta_{w,i,j}^{k+1}=\left\{\begin{array}{l}2\bar{\alpha}\theta_{w,i+1,j}+\dfrac{\bar{\alpha}}{\bar{\varepsilon}^2}\Phi^2\theta_{w,i,j+1}+\\ \dfrac{\bar{\alpha}}{\bar{\varepsilon}^2}\Phi^2\theta_{w,i,j-1}-2\bar{\alpha}\left(1+\dfrac{\Phi^2}{\bar{\varepsilon}^2}\right)\theta_{w,i,j}-\\ 2\bar{\alpha}\Delta\chi F_{wx1}\end{array}\right\}\Bigg/2\bar{\alpha}\left(1+\frac{\Phi^2}{\bar{\varepsilon}^2}\right) \qquad (24)$$

where $F_{wx1}=\left(\partial\theta_w/\partial\chi\right)\big|_{\chi=0}=0$, for $i=0; j=1$ to *jmax - 1.*

In the same way, the boundary condition at the right side of the microchannel wall gives

$$\Delta\theta_{w,i,j}^{k+1}=\left\{\begin{array}{l}2\bar{\alpha}\theta_{w,i-1,j}+\dfrac{\bar{\alpha}}{\bar{\varepsilon}^2}\Phi^2\theta_{w,i,j+1}+\\ \dfrac{\bar{\alpha}}{\bar{\varepsilon}^2}\Phi^2\theta_{w,i,j-1}-2\bar{\alpha}\left(1+\dfrac{\Phi^2}{\bar{\varepsilon}^2}\right)\theta_{w,i,j}+\\ 2\bar{\alpha}\Delta\chi F_{wx2}\end{array}\right\}\Bigg/2\bar{\alpha}\left(1+\frac{\Phi^2}{\bar{\varepsilon}^2}\right) \qquad (25)$$

where $F_{wx2}=\left(\partial\theta_w/\partial\chi\right)\big|_{\chi=1}=0$, for $i=imax; j=1 \text{to } jmax - 1.$

The specified temperature in the internal interface of the microchannel wall as boundary condition from equation (13) is

$$\theta_w(i,j)=\theta(i,j), \text{ for } j=0, i=0 \text{ to } imax \qquad (26)$$

In addition to equation (13) was considered the condition marked by the equation (8) in the internal interface of the microchannel wall, with help from equation (26) is evaluated the following

$$\frac{\bar{\alpha}}{\bar{\varepsilon}^2}\frac{\partial\theta_{w,i,j}}{\partial Z}\Big|_{Z=0}=\frac{\bar{\alpha}}{\bar{\varepsilon}^2}\left(\frac{\theta_{w,i,j+1}-\theta_{w,i,j}}{\Delta Z}\right)=\frac{\partial\theta_{i,j}}{\partial\eta}\Big|_{\eta=1} \qquad (27)$$

The previous equation is necessary to evaluate $F_{y2(i,j)}$ in the equation (22) for the fluid region.

Now, the boundary condition at the external interface of the microchannel wall gives

$$\Delta\theta_{w,i,j}^{k+1}=\left\{\begin{array}{l}\bar{\alpha}\theta_{w,i+1,j}+2\dfrac{\bar{\alpha}}{\bar{\varepsilon}^2}\Phi^2\theta_{w,i,j-1}+\bar{\alpha}\theta_{w,i-1,j}-\\ 2\bar{\alpha}\left(1+\dfrac{\Phi^2}{\bar{\varepsilon}^2}\right)\theta_{w,i,j}-2\Lambda\Phi^2\Delta Z\end{array}\right\}\Bigg/2\bar{\alpha}\left(1+\frac{\Phi^2}{\bar{\varepsilon}^2}\right) \qquad (28)$$

for $j=jmax, i=1$ to *imax - 1.*

The boundary conditions in the corner nodes $i=0,\ j=jmax$ and $i=imax,\ j=jmax$ are respectly adapted to the SOR method.

Equations (17), (19-20), (22), (23-25) and (28) are replaced in an iterative process in equation (16) for each node of the discretized mesh that is not specified temperature. The SOR method ends the process when the temperature converges at each node until $\Delta\theta_{i,j}^{k+1} \le tolerance = tol$. For the conjugate problem, we solved firstly the temperature field in the solid region with an arbitrary specified temperature in the internal interface to initialize the problem, then the temperature gradient in the internal interface of solid wall was calculated by the equation (27), and after it was taken to calculate the temperature gradient of fluid region in same equation (27); so with this, the temperature field in the fluid region was calculated. Once that the solid and fluid region are solved, we compare the calculated interfacial temperature by $\left|\theta(i,j)\right|_{\eta=1} - \theta_w(i,j)\big|_{Z=0}\right| \le 0.001$, if the previous condition is not satisfied, then the cycle is repeated with the new calculated interfacial temperature in the solid $\theta_w\big|_{z=0} = \theta\big|_{z=0}$. To implement the discretized mathematical model was used the programming software Fortran Power Station 4.0 and the following parameter values: $\Delta\chi$*=0.005,* $\Delta\eta$*=0.005,* ΔZ*=0.005, imax=200, jmax=200, tol=*10^{-8}.

D. Asymptotic solution

An analytical solution was considering in the limit where the parameter $\bar{\alpha}$ is small, to this form was proposed the following expansion to fluid temperature

$$\theta = \theta_0(\chi) + \bar{\alpha}\theta_1(\chi,\eta) + ... \tag{29}$$

and for the solid temperature

$$\theta_w = \theta_{w0}(\chi,Z) + \bar{\alpha}\theta_{w1}(\chi,Z) + ... \tag{30}$$

Substituting the equation (29) into (6)

$$\beta Pe\bar{u}\left[\frac{\partial\theta_0}{\partial\chi} + \bar{\alpha}\frac{\partial\theta_1}{\partial\chi} + ...\right] = \beta^2\left[\frac{\partial^2\theta_0}{\partial\chi^2} + \bar{\alpha}\frac{\partial^2\theta_1}{\partial\chi^2} + ...\right] + \bar{\alpha}\frac{\partial^2\theta_1}{\partial\eta^2} + 1 \tag{31}$$

Comparing in orders of magnitude the diffusive terms with the energy generation term in the equation (1), is showed that the significant temperature variations occur in the axial coordinate, then we can integrate and simplifying the equation (31) in the transversal direction

$$\begin{aligned}&\beta Pe\frac{\partial\theta_0}{\partial\chi}\int_{\eta=0}^{\eta=1}\bar{u}d\eta + \bar{\alpha}\beta Pe\frac{\partial\theta_1}{\partial\chi}\int_{\eta=0}^{\eta=1}\bar{u}d\eta = \\ &\beta^2\frac{\partial^2\theta_0}{\partial\chi^2}\int_{\eta=0}^{\eta=1}d\eta + \bar{\alpha}\beta^2\frac{\partial^2\theta_1}{\partial\chi^2}\int_{\eta=0}^{\eta=1}d\eta + \bar{\alpha}\left.\frac{\partial\theta_1}{\partial\eta}\right|_{\eta=1} + 1\end{aligned} \tag{32}$$

Now, substituting the expansions from the equation (29) and (30) into (8) and simplifying

$$\frac{1}{\bar{\varepsilon}^2}\left[\left.\frac{\partial\theta_{w0}}{\partial Z}\right|_{Z=0} + \bar{\alpha}\left.\frac{\partial\theta_{w1}}{\partial Z}\right|_{Z=0}\right] = \left.\frac{\partial\theta_1}{\partial\eta}\right|_{\eta=1} \tag{33}$$

For collecting the zero power of $\bar{\alpha}$ from equation (33), we get

$$O(\alpha^0): \frac{1}{\bar{\varepsilon}^2}\left.\frac{\partial\theta_{w0}}{\partial Z}\right|_{Z=0} = \left.\frac{\partial\theta_1}{\partial\eta}\right|_{\eta=1} \tag{34}$$

By considering the limit in $\bar{\alpha} \ll 1$ and $\bar{\alpha}/\bar{\varepsilon}^2 \sim O(1)$ the temperature gradients in the microchannel wall are a constant and $\left(\partial\theta_w/\partial Z\right)\big|_{Z=1} = \left(\partial\theta_{w0}/\partial Z\right)\big|_{Z=0}$, in these conditions, substituting the equation (14) into (34) is obtained

$$\left.\frac{\partial\theta_1}{\partial\eta}\right|_{\eta=1} = -\frac{\Lambda}{\bar{\alpha}} \tag{35}$$

So, by substituting the equation (35) into (32) and collecting the zero power of $\bar{\alpha}$, we get

$$O(\alpha^0): \beta Pe\frac{\partial\theta_0}{\partial\chi}\int_{\eta=0}^{\eta=1}\bar{u}d\eta = \beta^2\frac{\partial^2\theta_0}{\partial\chi^2}\int_{\eta=0}^{\eta=1}d\eta - \Lambda + 1 \tag{36}$$

with the corresponding boundary conditions

$$\begin{aligned}&\chi = 0: \theta_0 = 0 \\ &\chi = 1: \partial\theta_0 \big/ \partial\chi = 0\end{aligned} \tag{37}$$

The solution in a first approximation to equation (36) is

$$\theta_0 = \frac{(\Lambda-1)\left[\exp\left(\frac{Pe\int_{\eta=0}^{\eta=1}\bar{u}d\eta}{\beta}(\chi-1)\right) - \exp\left(-\frac{Pe\int_{\eta=0}^{\eta=1}\bar{u}d\eta}{\beta}\right)\right]}{\left(Pe\int_{\eta=0}^{\eta=1}\bar{u}d\eta\right)^2} + \frac{(1-\Lambda)\chi}{\beta Pe\int_{\eta=0}^{\eta=1}\bar{u}d\eta} \tag{38}$$

In the solid region case was considered the limit $\bar{\alpha} \ll 1$, and $\bar{\alpha}/\bar{\varepsilon}^2 \sim O(1)$, then from equation (12)

$$\frac{\partial^2\theta_w}{\partial Z^2} = 0 \tag{39}$$

with the corresponding boundary conditions

$$Z = 0 : \theta = \theta_w \tag{40}$$

Therefore the analytical solution in a first approximation to the energy equation to solid region is

$$\theta_{w0}(\chi, Z) = -\frac{\bar{\varepsilon}^2}{\bar{\alpha}} \Lambda Z + \theta_0(\chi) \tag{41}$$

RESULTS AND DISCUSSIONS

In this study, we consider the order of magnitude of the following characteristic values: $H \sim 10^{-4}\, m$ [1,9], $H_w \sim 10^{-5}\, m$ [7,8,9], $L \sim 10^{-2} m$ [6,8]; $\bar{\kappa} = 100$, based in a 0.001 mM buffer solution and symmetrical electrolyte [3]; therefore $\beta \sim 0.01$ and $\bar{\varepsilon} \sim 0.001$. Thermal properties of materials were taken as $k_f = 0.61 - 0.7 W/m \cdot K$ for the fluid, $k_w = 0.15 - 0.19$ $W/m \cdot K$ for PMMA polymer wall and $k_w = 1.38 W/m \cdot K$ for fused silica wall [6, 9], therefore $\bar{\alpha} \sim 2.5x10^{-6} - 2.5x10^{-5}$; $\sigma \sim 10^{-3} - 10^{-2}\ S/m$; $u_{HS} \sim 10^{-4} - 10^{-3}$ [19], $\epsilon \sim 10^{-10} C/m \cdot V$, $\zeta \leq 10^{-2} V$, $E_x \sim 10^4 - 10^5\ V/m$ [3] and $\eta_0 \sim 10^{-3} - 10^{-4}$ $Pa \cdot s$ [8, 12, 20], $\rho \sim 10^3$ kg/m^3, $C_p = 4180$ J/kgK [6]; therefore $Pe \sim 0.5 - 1.5$ [20]; $-1 \leq \Gamma \leq 2.5$ [17]; $\varepsilon De_\kappa^2 = 0, 1, 4$ [17]; $\Lambda = 1, 0.75, 0.5$ [12].

The Figure 2 shows the spatial development of the Joule heating induced to the fluid and wall temperature fields in the microchannel along *y* direction in the middle axial position. The temperature distributions in the fluid region exhibit a parabolic-like pattern while the solid wall exhibits a linear behavior [9]. It also shows that the highest temperature occurs at the microchannel centerline; for that is clear that the heat generated by Joule heating is transferred from the central region to wall by convection and conduction in the fluid, and dissipated though the microchannel wall by conduction, finally the heat is transferred to the exterior by the q_0''. For the parameters shown in the Figure 2 we can see that for the increases of viscoelastic parameter εDe_κ^2 the velocity also increases [17], causing an important decrease in temperature by the effect of convection. To $\varepsilon De_\kappa^2 = 0$ the Newtonian case is recovered.

For the parameters shown in the Figure 3, the influence of the ratio of pressure forces on electro-osmotic forces Γ is relevant, because for negative values of $\Gamma = -1$ acts a drag increaser on the flow, decreasing the temperature profiles of system by the increase of the velocity, increasing the convective effects. On the other hand, for positive values of $\Gamma = 2.5$, its acts a drag reducer on the flow therefore causing an increase of temperature profiles by the decrease of velocity, decreasing the convective effects. Then $\Gamma < 0$ and $\Gamma > 0$ correspond to Poiseuille electro-osmotic flows with favorable and adverse pressure gradients, respectively. For $\Gamma = 0$ the velocity profiles correspond to a pluglike flow, due to the solely action of electroosmotic forces [17].

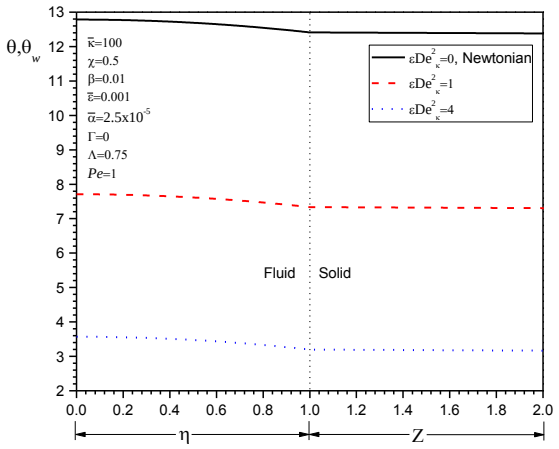

FIG. 2 SPATIAL DEVELOPMENT OF TEMPERATURE PROFILES IN THE FLUID AND SOLID REGION ALONG TRANSVERSAL DIRECTION FOR DIFFERENT VALUES OF VISCOELASTIC PARAMETER εDe_κ^2.

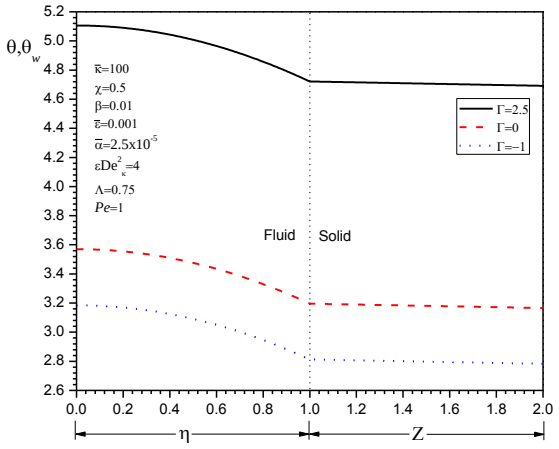

FIG. 3 SPATIAL DEVELOPMENT OF TEMPERATURE PROFILES IN THE FLUID AND SOLID REGION ALONG TRANSVERSAL DIRECTION FOR DIFFERENT VALUES OF THE RATIO OF PRESSURE FORCES ON ELECTRO-OSMOTIC FORCES Γ.

The Figure 4 shows the spatial development of the temperature profiles along transversal direction to the fluid and solid region, and to different axial positions. For the parameters shown, there is a constant increase of Joule heating toward the outlet of the microchannel [21]. The Figure 5 exhibit the influence of the thermal properties in the heat transfer phenomena because by comparing the material of fused silica solid wall with $\bar{\alpha} \sim 2.5x10^{-5}$ versus PMMA polymer wall with $\bar{\alpha} \sim 2.5x10^{-6}$,

we can find the thermal conductivity of PMMA is much lower than that of silica glass. This mean the heat dissipation trough the PMMA wall is more difficult than through the glass wall, leaving an important temperature changes in solid region [9]. Then for decrease the value of $\bar{\alpha}$ the temperature gradient in the solid region tend to increase by the decrease of conduction effect.

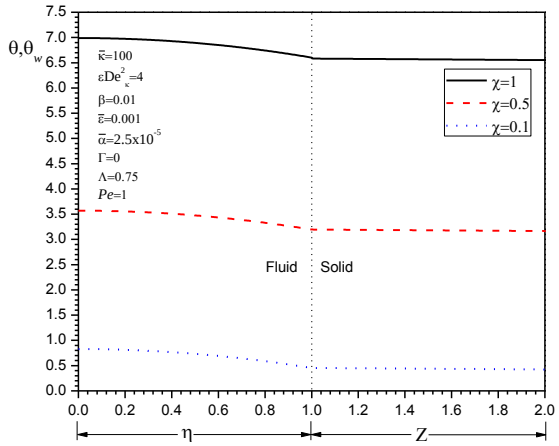

FIG. 4 SPATIAL DEVELOPMENT OF TEMPERATURE PROFILES IN THE FLUID AND SOLID REGION ALONG TRANSVERSAL DIRECTION FOR DIFFERENT AXIAL POSITIONS χ .

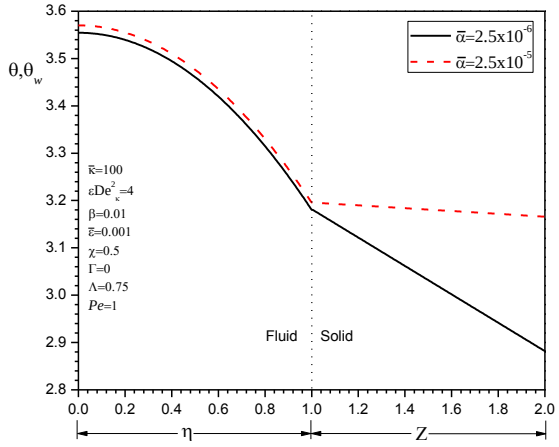

FIG. 5 SPATIAL DEVELOPMENT OF TEMPERATURE PROFILES IN THE FLUID AND SOLID REGION ALONG TRANSVERSAL DIRECTION FOR DIFFERENT CONJUGATION TERM $\bar{\alpha}$.

The Figure 6 shows that for decrease of *Pe* number the convection effect decrease over conduction effect, increasing the temperature profiles significantly. So the *Pe* number is an indicator of the convection velocity in the system.

The Figure 7 depicts the temperature profiles across transversal direction of microchannel in the middle axial length for the fluid and solid region, for $\Lambda = 1, 0.75, 0.5$. In all cases the value of q_0'' is considered as an extraction of heat from the channel walls. Is important recall here that the temperature rises in electro- osmotic flows under constant wall heat flux boundary conditions, may attributed to the combined mechanism of Joule heating and heat transfer in the walls. For the cases studied in the Figure 7, the Joule heating seems to be a dominant mechanism behind temperature increments within the system. In general, for increase the value of q_0'', the transversal temperature tends to decrease, to a same contribution of Joule heating. So, from the different temperature profiles we can see that the lower value of Λ, higher is the temperature rise at a given axial location of the microchannel [12].

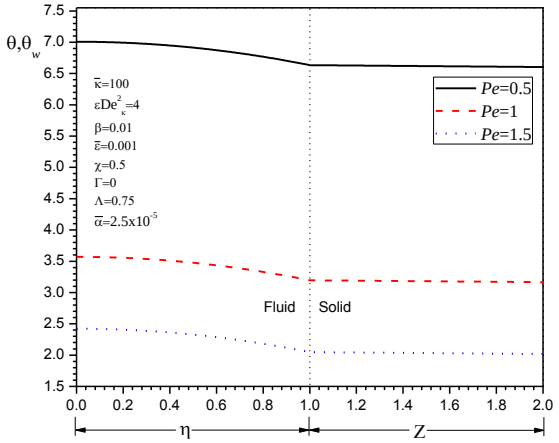

FIG. 6 SPATIAL DEVELOPMENT OF TEMPERATURE PROFILES IN THE FLUID AND SOLID REGION ALONG TRANSVERSAL DIRECTION FOR DIFFERENT *Pe* NUMBER.

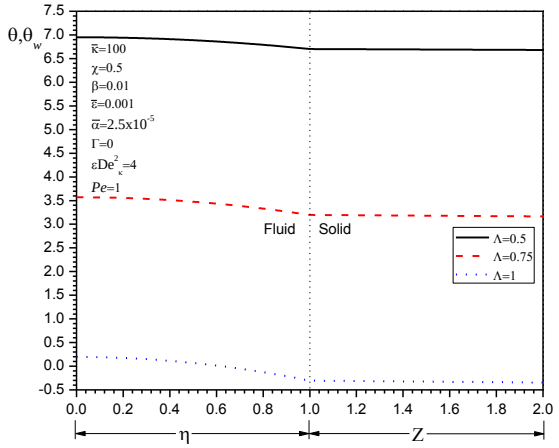

FIG. 7 SPATIAL DEVELOPMENT OF TEMPERATURE PROFILES IN THE FLUID AND SOLID REGION ALONG TRANSVERSAL DIRECTION FOR DIFFERENT RATIO OF HEAT FLUX FROM THE EXTERNAL WALL TO THE JOULE HEATING Λ .

In order to validate the numerical solution from the equations (6-8), the Figure 8 compares the behavior of the axial temperature profile in the fluid region with the asymptotic

solution given by equation (38). We can see that, the first approximation for the asymptotic solution is near to the predictions of the axial temperature profile for the fluid region in the numerical solution for three different transversal positions $\eta = 0, 0.5, 1$ along the microchannel.

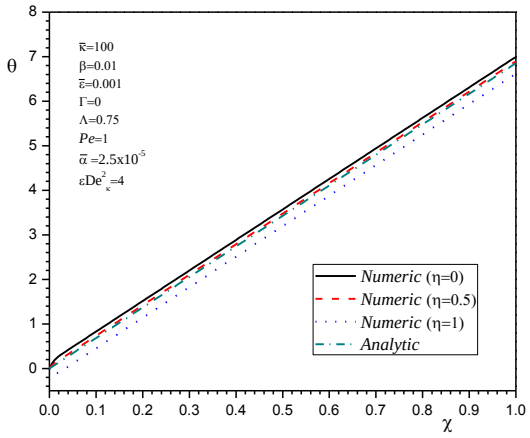

FIG. 8 COMPARISON OF THE NUMERICAL AND ANALYTIC SOLUTION FOR THE SPATIAL DEVELOPMENT OF TEMPERATURE PROFILES IN THE FLUID ALONG AXIAL DIRECTION.

The Figure 9 compares the behavior of the transversal temperature profile in the solid region given from the equations (8, 12-14) with the asymptotic solution given by equations (41). We can see the first approximation for the asymptotic solution of the temperature profile for the solid region with the numerical solution in the middle axial position in the microchannel.

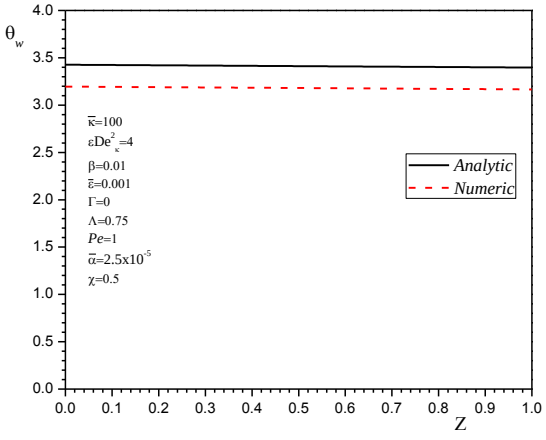

FIG. 9 COMPARISON OF THE NUMERICAL AND ANALYTIC SOLUTION FOR THE SPATIAL DEVELOPMENT OF TEMPERATURE PROFILES IN THE SOLID ALONG TRANSVERSAL DIRECTION.

CONCLUSIONS

The present work analyzed different transport characteristics of mixed electro-osmotic and pressure driven flows of non Newtonian fluids, at the same time helps to understand the consequences of the interaction between the applied electric field within the EDL and the result of temperature increase by Joule heating, which has important effects of practical significance. Such Joule heating effects can be significant consequences in low column separation efficiency, reduction of analysis resolution, or even loss of injected samples in biomedical applications. So, the present model can act as a tool towards understanding of the different interconnected transport mechanisms in the efficient design of microfluidic systems.

ACKNOWLEDGMENTS

This work was supported by a grant 58817 SEP-CONACYT and 20100552 SIP-IPN at Mexico.

NOMENCLATURE

C_p	specific heat [J/kg K]
D	constant simplification
De_κ	Deborah number based on the thickness of the EDL and the Helmholtz-Smoluchowski velocity
E_x	electric field along the axis of the microchannel [V/m]
F	simplified variable
F_{wx1}	temperature gradient in the left side of microchannel wall
F_{wx2}	temperature gradient in the right side of microchannel wall
F_{x2}	temperature gradient in the outlet of microchannel
F_{y1}	temperature gradient in the center of microchannel
$F_{y2(i,j)}$	temperature gradient in the internal interface of microchannel
H	half of microchannel [m]
H_w	wall thickness of the microchannel [m]
$imax$	maximum numbers of nodes in the axial coordinate
$jmax$	maximum numbers of nodes in the transversal coordinate
k	thermal conductivity [W/m-K]
L	length of microchannel [m]
M	constant simplification
p_x	pressure gradient in axial direction [N/m^2]
Pe	Peclet number
q''_0	heat flux at the wall in the region $0 \le x \le L$ [W/m^2]
R	simplified variable
T	temperature [K]
T_e	microchannel inlet temperature [K]
u	fluid axial velocity [m/s]
$\bar{u}$	dimensionless fluid axial velocity
u_{HS}	reference electro-osmotic velocity [m/s]
w	depth of the microchannel [m]
x	axial coordinate [m]
y	transversal coordinate [m]

Greek symbols

$\bar{\alpha}$	conjugation term
β	aspect ratio of the fluid region
Γ	ratio of pressure forces on electro-osmotic forces
$\Delta\eta$	increment in the transversal direction of fluid
$\Delta\theta$	dimensionless temperature variation in the fluid region
$\Delta\theta_w$	dimensionless temperature variation in the solid region
$\Delta\chi$	increment in the axial direction of fluid and solid
ΔZ	increment in the transversal direction of solid
ε	coefficient of elongational viscosity
$\bar{\varepsilon}$	aspect ratio of the solid region
Z	dimensionless transversal coordinate of the solid wall
ζ	Zeta potential in the shear plane of the EDL [V]
η	dimensionless transversal coordinate of the fluid region
η_0	apparent viscosity [Pa-s]
θ	dimensionless fluid temperature
θ_w	dimensionless solid temperature
κ	inverse Debye length [m^{-1}]
$\bar{\kappa}$	electrokinetic parameter
Λ	ratio of heat flux from the external wall to the Joule heating
λ_1	relaxation time [s]
ρ	fluid density [kg/m^3]
σ	electrical conductivity of the fluid [S/m]
Φ	aspect ratio of the mesh in the solid
χ	dimensionless axial coordinate
Ω	aspect ratio of the mesh in the fluid
ϖ	relaxation factor of SOR method

Other symbols

$\in$	dielectric constant [C/V-m]

Subscripts

f	fluid
i	nodal position in the axial direction
j	nodal position in the transversal direction
w	wall

superscripts

k	iteration

REFERENCES

[1] Tang G., Yan D., Yang C., Gong H., Chai C. and Lam Y., 2007, "Joule heating and its effects on electrokinetic transport of solutes in rectangular microchannels", Sensors and Actuators A, **139**, pp. 221–232.

[2] Zhao C., Zholkovskij A., Masliyah J. H. and Yang C., 2008, "Analysis of electroosmotic flow of power – law fluids in a slit microchannel". Journal of Colloid and Interface Science, **326**, pp. 503-510.

[3] Masliyah J. H., Bhattacharjee S., 2006, *Electrokinetic and Colloid Transport Phenomena*, Wiley Interscience, Chap. 4 – 7.

[4] Karniadakis G., Beskok A., Aluru N., 2005, *Microflows and Nanoflows*. Interdiciplinary Applied Mathematics, Springer, V. 29, Chap. 7.

[5] Li D., 2004, *Electrokinetics in Microfluidics*. Interface Science and Technology, Elsevier Academy Press, V. 2.

[6] Xuan X., Sinton D., Li D., 2004, "Thermal end effects on electroosmotic flow in a capillary", International Journal of Heat and Mass Transfer, **47**, pp. 3145–3157.

[7] Xuan X., Xu B., Sinton D. and Li D., 2004, "Electroosmotic flow with Joule heating effects", Miniaturisation for Chemistry, Biology & Bioengineering Lab Chip, **4**, pp. 230 – 236.

[8] Tang G. Y., Yang C., Chai J.C., Gong H.Q., 2004, "Joule heating effect on electroosmotic flow and mass species transport in microcapillary". International Journal of Heat and Mass Transfer, **47**, pp. 215–227.

[9] Tang G. Y., Yang C., Chai C. K., and Gong H. Q., 2004, "Numerical analysis of the thermal effect on electroosmotic flow and electrokinetic mass transport in microchannels", Analytica Chemica Acta, **507**, pp. 27 -37.

[10] Tang G. Y., Yang C., Chai C. J., and Gong H. Q., 2003, "Modeling of electroosmotic flow and capillary electrophoresis with the Joule heating effect: the Nerts – Plank equation versus the Boltzmann distribution", Langmuir, **19**, pp. 10975-10984.

[11] Xuan X. and Li D., 2005, "Analytical study of Joule heating effects on electrokinetic transportation in capillary electrophoresis", Journal of Chromatography A, **1064**, pp. 227 - 237.

[12] Das S., Chakraborty S., 2006, "Analytical solutions for velocity, temperature and concentration distribution in electroosmotic microchannel flows of a non-Newtonian bio-fluid", Analytica Chimica Acta, **559**, pp. 15-24.

[13] Zhao C., Zholkovskij E., Masliyah J. H., Yang C., 2008, "Analysis of electroosmotic flow of power – law fluids in a slit microchannel", Journal of Colloid and Interface Science, **326**, pp. 503-510.

[14] Berli C. L. A., Olivares M. L., 2008, "Electrokinetic flow of non-Newtonian fluids in microchannels", Journal of Colloid and Interface Science, **320**, pp. 582-589.

[15] Tang G. H., Li X. F., He Y. L., Tao W. Q., 2009, "Electroosmotic flow of non-Newtonian fluid in microchannels", Journal of Non-Newtonian Fluid Mechanics, **157**, pp. 133-137.

[16] Park H. M. and Lee W. M., 2008, "Helmholtz – Smulochowski for viscoelastic electroosmotic flows", Journal of Colloid and Interface Science, **317**, pp. 631-636.

[17] Alfonso A. M., Alves M. A., Pinho F. T., 2009, "Analytical solution of mixed electro-osmotic/pressure driven flows of viscoelastic fluids in microchannels", Journal of Non-Newtonian Fluid Mechanics, **159**, pp. 50-63.

[18] Hoffman J. D., 2001, *"Numerical Methods for Engineers and Scientist"*, Marcel Dekker, Inc., Chap. 5, 9.

[19] Ramos A, 2007, *"Electrohydrodyanamics and Magnetohydrodynamics Micropumps"*, Microfluidic Technologies for Miniaturized Analysis Systems, Springer US, Chap 2.

[20] Horiuchi K., Dutta P., 2004, "Joule heating effects in electroosmotically driven microchannel flows", International Journal of Heat and Mass Transfer, **47**, pp. 3085–3095.

[21] Horiuchi K., Dutta P. and Hossain A., 2006, "Joule-heating effects in mixed electro-osmotic and pressure-driven microflows under constant wall heat flux", Journal of Engineering Mathematics, **54**, pp. 159–180.